

**AUTHOR(S):**

**TITLE:**

**YEAR:**

**Publisher citation:**

**OpenAIR citation:**

**Publisher copyright statement:**

This is the \_\_\_\_\_ version of an article originally published by \_\_\_\_\_  
in \_\_\_\_\_  
(ISSN \_\_\_\_\_; eISSN \_\_\_\_\_).

**OpenAIR takedown statement:**

Section 6 of the “Repository policy for OpenAIR @ RGU” (available from <http://www.rgu.ac.uk/staff-and-current-students/library/library-policies/repository-policies>) provides guidance on the criteria under which RGU will consider withdrawing material from OpenAIR. If you believe that this item is subject to any of these criteria, or for any other reason should not be held on OpenAIR, then please contact [openair-help@rgu.ac.uk](mailto:openair-help@rgu.ac.uk) with the details of the item and the nature of your complaint.

This publication is distributed under a CC \_\_\_\_\_ license.

\_\_\_\_\_

# A laboratory study of rail–wheel interaction monitoring using acoustic emission: effect of rolling conditions with and without lateral rattling

Proc IMechE Part F:  
*J Rail and Rapid Transit*  
0(0) 1–15  
© IMechE 2012  
Reprints and permissions:  
sagepub.co.uk/journalsPermissions.nav  
DOI: 10.1177/0954409712458497  
pif.sagepub.com  


2

Nirav A Thakkar, John A Steel and Robert L Reuben

## Abstract

This paper presents part of an extended laboratory study on the potential to apply the acoustic emission (AE) technique for in-situ rail–wheel interaction monitoring using rail-mounted sensors. The essential monitoring principle is that the intensity of the rail–wheel contact will affect the intensity of the AE that is generated during rolling. The current paper is confined to situations of ‘normal’ rolling, investigating the effects of wheel load, speed and lateral rattling of the generated AE, although the wider study includes the effects of rail and wheel irregularities on the AE generated. Rail–wheel contact was simulated on a scaled test rig consisting of a single wheel rolled round a circular track using a motor mounted at the centre of the track attached to a driving arm. AE was recorded at a fixed point on the track while the wheel was rolled around the track at a range of speeds with varying axle load. Wheel slip was found to be insignificant and tests using a simulated source confirmed that the energy recorded with a source at a given position on the track was repeatable. In one set of experiments, measures were taken to eliminate lateral rattling of the wheel and eccentricity of the wheel arc relative to the track arc. In a second set of experiments, some lateral float of the wheel along the axle was allowed and a limited amount of eccentricity was built into the track. The energy per wheel rotation for normal rolling was found to increase in a linear fashion with increasing axle load and centrifugal force, as would be expected due to the increasing rolling resistance with axle load and increasing lateral force with angular speed. The frictional instability associated with the lateral rattling was clearly detectable at low axle loads and lower speeds, and both natural and eccentricity (flange rubbing) rail abnormalities were detectable in the AE record. It is concluded that, with appropriate calibration, contact stresses between wheel and rail on straight or curved track can be monitored using track-mounted sensors so that cumulative contact stress can potentially be monitored.

## Keywords

Acoustic emission, rail–wheel interaction, stress intensity monitoring

Date received: 28 August 2011; accepted: 12 July 2012

## Introduction

Rail–wheel interaction remains a subject of considerable current interest to both track design and track maintenance engineers, and the importance of way-side monitoring in providing further design and maintenance information has recently been highlighted.<sup>1</sup> Vertical wheel load is a major factor in most of the main rail deterioration mechanisms including track settlement, fatigue of components (such as points, fasteners, pads and sleepers), wear and rolling contact fatigue (RCF). Vertical wheel load is related to axle load, but will be dynamically amplified roughly in proportion to speed, with frequencies in the tens of hertz range.<sup>2</sup> Much of the work on monitoring the dynamics of wheel–rail contact has been applied

noise reduction, and this work has revealed some very complex interactions between wheel and track roughness, rail and wheel stiffness, and track foundations, the overall effect being that noise is generated by rail and wheel vibrations in the frequency range from about 50 Hz to 2 kHz, although curve squeal is much less well-understood because the forcing

School of Engineering and Physical Sciences, Heriot-Watt University, UK

### Corresponding author:

Robert L Reuben, Mechanical Engineering, School of Engineering and Physical Sciences, Heriot-Watt University, Riccarton, Edinburgh, EH14 4AS, UK.

Email: R.L.Reuben@hw.ac.uk

function is believed to be frictional instability rather than roughness-induced vertical displacements.<sup>3</sup> Given this complex loading situation, traditional mean gross tonnage (MGT)-based rail life prediction methods are not reliable since dynamic loading produces non-uniform and dynamic stress distributions from traction, braking and steering forces, often giving rise to multipoint contact pressure distributions rather than the Hertzian distribution traditionally assumed.<sup>4</sup> Both wear and RCF models include contact forces (see, for example, Tunna et al.<sup>5</sup>) and such models are now used in the management of rail assets using parameters estimated from wheel and track geometry, axle loads and speed.<sup>6, 7</sup> The object of the current work is to assess whether the intensity of rail-wheel contact can be monitored using acoustic emission (AE) in much the same way as fatigue forcing parameters are monitored in other civil engineering assets, such as wave loading in ships.<sup>8</sup>

The American Railway Engineering and Maintenance-of-Way Association guidance on rolling friction in rails<sup>9</sup> suggests that the track resistance,  $F$ , (as a force) is given by:  $F = A + Bv$ , where  $v$  is the train speed, the speed-independent component,  $A = A_1 + A_2/W$ , depends on axle load,  $W$ , and includes rolling resistance and track resistance, and the speed-dependent component,  $B$ , includes flange friction, flange impact, rolling resistance and waviness in the rail. Track stiffness plays an important part in determining track rolling resistance, less stiff tracks producing more resistance for a given axle load. Lukaszewicz<sup>10</sup>, working from the point of view of energy consumption in rail haulage, has measured the mechanical rolling resistance of ore trains and has found the curve resistance to be

$$F_{Mc} = \frac{a}{R-b} \sum_{i=1}^{n_c} W_i$$

where  $a$  and  $b$  depend on the train and/or wagon types,  $R$  is the radius of curvature,  $n_c$  is the number of axles in the curve at a given time and the  $W_i$  are the weights of the wagons. In addition the tangent track resistance was found to be

$$F_{Mt} = A + Bv = \sum_{i=1}^{n_{ax}} (c + d \times W_i) + e \times L_T \times v$$

where  $c$ ,  $d$  and  $e$  depend on the train and/or wagon types,  $n_{ax}$  is the number of axles and  $L_T$  is the length of the train. Lukaszewicz used the train length to modify  $B$  as he did not find it to depend on axle load, a fact that he interpreted as it being associated with air momentum drag rather than rolling resistance. He also noted, for the relatively stiff tracks in his study, that  $B$  accounted for rather a small proportion of overall energy consumption, although this does not acknowledge that speed will affect the dynamic loading of the track and hence rolling

resistance. Zeng and Wu<sup>11</sup> have also identified two components of lateral force in canted curves

$$F_{gi} = m_i \frac{v^2}{R} \cos \alpha - m_i g \sin \alpha$$

where  $m$  is the mass of the relevant body and  $\alpha$  is the cant angle of the outer rail.

Tournay<sup>1</sup> has recognized two extremes in a continuum of degradation mechanisms, the wear regime and the stress regime, and has suggested that the latter is the one requiring more attention from tribologists. He also identified wayside detection of vehicle performance as being a key to the identification of the worst performing trains in order to reduce cumulative stresses. Increasing contact stress not only increases wear, but also increases the rate of surface-breaking crack growth<sup>12</sup> as well as the rate of RCF crack growth.<sup>13</sup> Thus, being able to monitor, in a given area of track, the evolution of stress range with time will, in principle, allow cumulative damage according to the Paris law<sup>14</sup> to be monitored to complement purely statistical approaches based on MGT.<sup>15</sup>

Papaelias et al.<sup>16</sup> have recently reviewed the state-of-the-art of rail non-destructive evaluation, mostly from the point of view of methods used to locate rail defects, although they do mention a technique which uses wheel-mounted microphones to measure airborne sound, indicating that it measures 'acoustic track quality' and can detect 'certain defects'. The position and size of the wheel-rail contact patch has been measured in the laboratory using scanned, focused active ultrasound probes (see, for example, Pau and Leban<sup>17</sup>). Although this approach is probably most useful for validating simulations of contact mechanics, use of a track-mounted phased array embedded at critical areas of track has been envisaged.<sup>17</sup> Other techniques for rail-wheel interaction quality measurement include an optical approach where the wheel and rail profiles are measured online to obtain a measure of the equivalent conicity.<sup>18</sup> The main disadvantage of this approach is that it needs to make a measurement on both wheel and rail and is only suitable for use with a specialist car.

The approach suggested in the current work is to use the active nature of AE monitoring to assess the level of contact stress intensity ( $\Delta\sigma$  and hence  $da/dn$  in the Paris law). AE monitoring is more sensitive than acceleration monitoring in this respect, because it is not sensitive to whole-body movement, but rather measures the elastic waves generated by the impacts and deformations produced in the contact zone, as has been established, for example, in the closely related application of rolling bearing monitoring.<sup>19</sup> In addition to the current paper, only Bruzelius and Mba<sup>20</sup> have assessed this application of AE, and they were only able to demonstrate that AE activity could be picked up in a laboratory rig. The current authors

have already observed discrete AE associated with the wheel-sets on a real train<sup>21</sup>, and, in a series of laboratory studies, have developed a moving source model for a rolling wheel<sup>22</sup> and have shown that natural rail defects<sup>23</sup> and simulated wheel defects<sup>24</sup> can be detected using AE monitoring. This paper demonstrates that AE can be used to assess the rolling conditions with and without lateral rattling and flange rubbing, thus providing the potential for track-side monitoring of cumulative fatigue damage.

## Experimental setup

The test rig consisted of a circular track around which a single wheel was rolled using a centrally mounted motor. The wheel assembly was mounted on a supporting arm, which was attached to the motor shaft at the centre of the test rig (Figure 1). Since the purpose of the experiments was to examine the effects of rolling conditions, no attempt was made to scale the rig dynamically as has been done by other investigators (see, for example, Armstrong and Thompson<sup>25</sup>). Instead, wheel surface speed and nominal (Hertzian) contact stress were maintained at the values pertaining to real trains. European trains travel at around 145 km/h (40 m/s) on wheels of diameter 900 mm, corresponding to tangential speeds of 4 m/s on the 90 mm diameter model wheel. Thus, the motor and gearbox were chosen to provide speeds of between 1 and 4 m/s, in increments of 0.5 m/s. The load per wheel on a rail passenger vehicle lies between 4.7 and 7.4 tonnes/wheel and around 11 tonnes/wheel for a freight wagon (CJC Jones, 2006, personal communication). The rail-wheel contact stresses (according to a model given by Pilkey<sup>26</sup>) corresponding to these forces are 880, 1030 and 1190 MPa, which, for the rail and wheel dimensions in the test rig, correspond to loads of 25,

41 and 62 N. The weight of the supporting arm and wheel assembly was 4 kg and a set of weights (two dead weights of 1 kg and one of 0.5 kg) were used to apply load incrementally up to a maximum of 6.5 kg (Figure 1). No lubricant was used on the track or wheels and no significant wear was found to occur over the timescale of the tests. Control tests at the commencement and end of the systematic experiments confirmed that no significant change had occurred in the AE records that could be attributed to changes in the rail-wheel contact conditions caused by wear or running-in.

It was important to determine if the wheel was always rolling under the conditions of load and speed investigated. To do this, scale markers were drawn onto the wheel and a section of rail (Figure 2) and a high-speed camera (Kodak Motion-Coder) was used to record the wheel passing the scaled length of track. Data were recorded at 400 frames per second for four different wheel speeds (1.5, 2, 3 and 3.5 m/s) and four different loads (4, 5, 6 and 6.5 kg). For each condition, four records were made over a fixed distance of 0.3 m, and angular and linear progress were measured as a function of time, one example result being shown in Figure 2. As can be seen, angular and linear progression were both regular, suggesting that no slip had occurred even at the highest speed and load. No evidence of slip was found in any of the records.

The measurement sensor was installed and demounted at its position shown in Figure 1 a total of 13 times, five pencil-lead breaks being performed close to the trigger sensor to establish the repeatability of AE energy measurement for a given installation of a given sensor. Figure 3 shows the AE energy recorded for each of the 65 pencil-lead breaks. As can be seen, the energy recorded within a given installation can

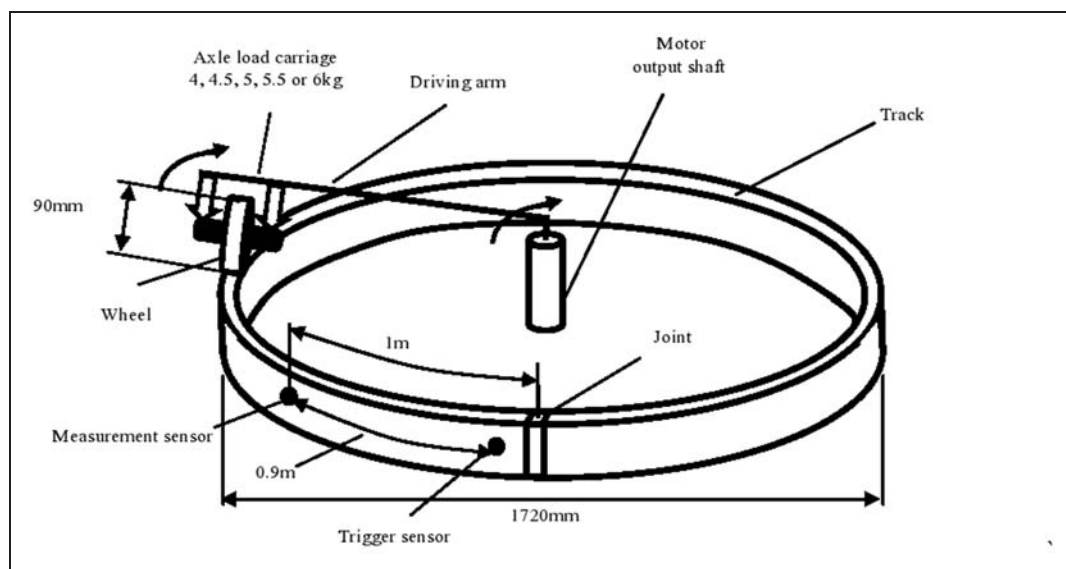
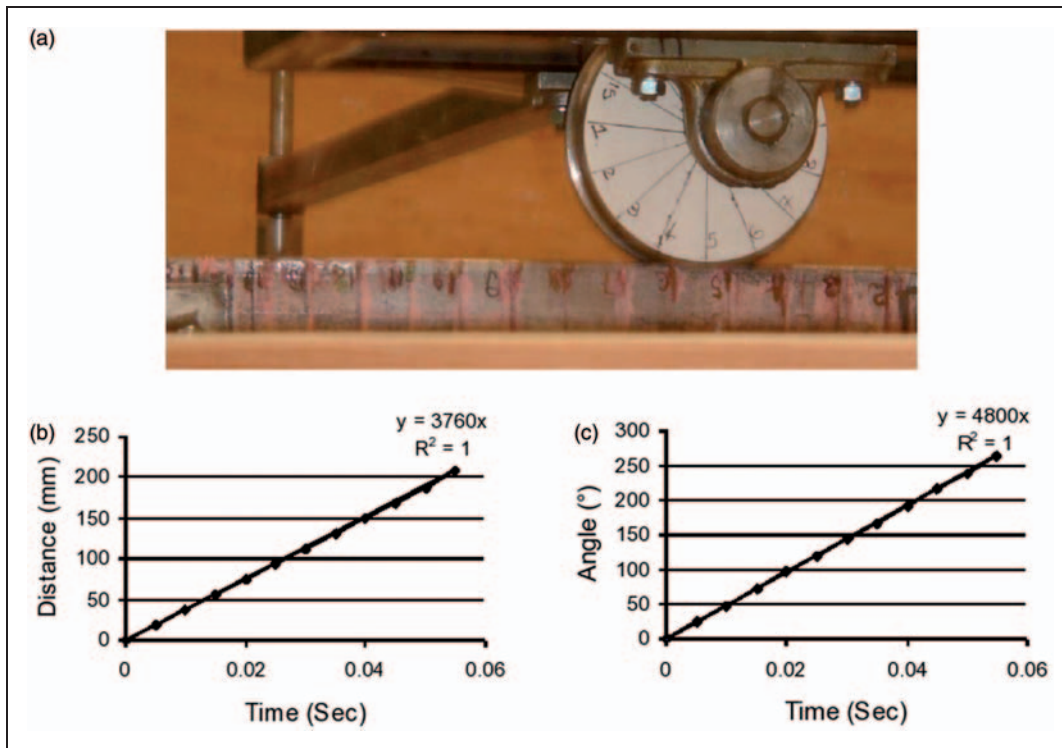
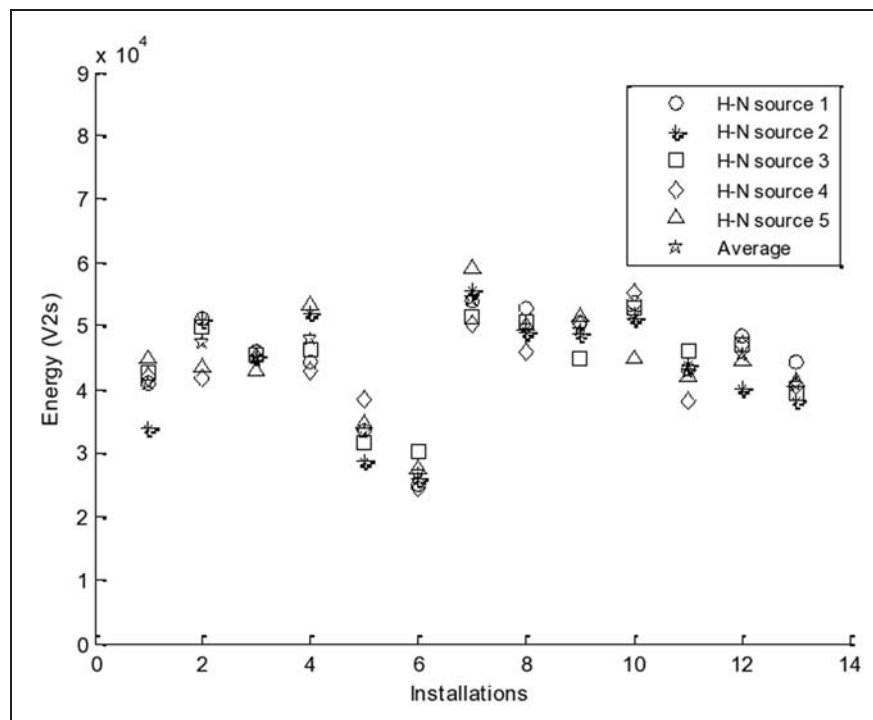


Figure 1. Experimental setup.



**Figure 2.** Arrangement for slip detection and high-speed camera results for a wheel speed of 3.5 m/s and 6.5 kg axle load: (a) marked wheel and track; (b) track distance travelled against time; and (c) wheel rotation angle against time.



**Figure 3.** Sensor installation repeatability test.

vary by about  $\pm 10\%$  and this can be attributed to variation of the pencil-lead break whereas that between installations (associated with the coupling) can vary by about  $\pm 20\%$ .

The experiments consisted of acquiring samples of unprocessed (raw) AE with the wheel rolling in various conditions. Data were acquired at 2.5 MHz, for 5,000,000 samples using the measurement sensor,

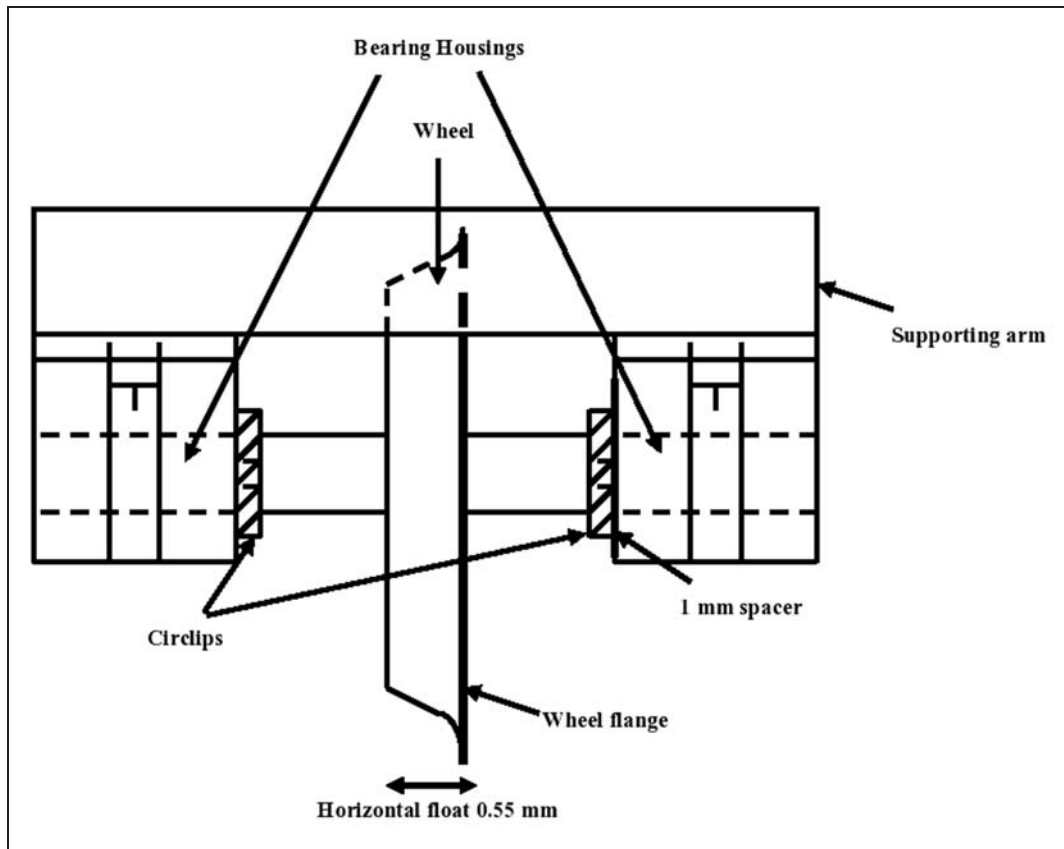


Figure 4. Schematic diagram of bearing housing, shaft and wheel assembly showing reduction in shaft play from 1.55 to 0.55 mm.

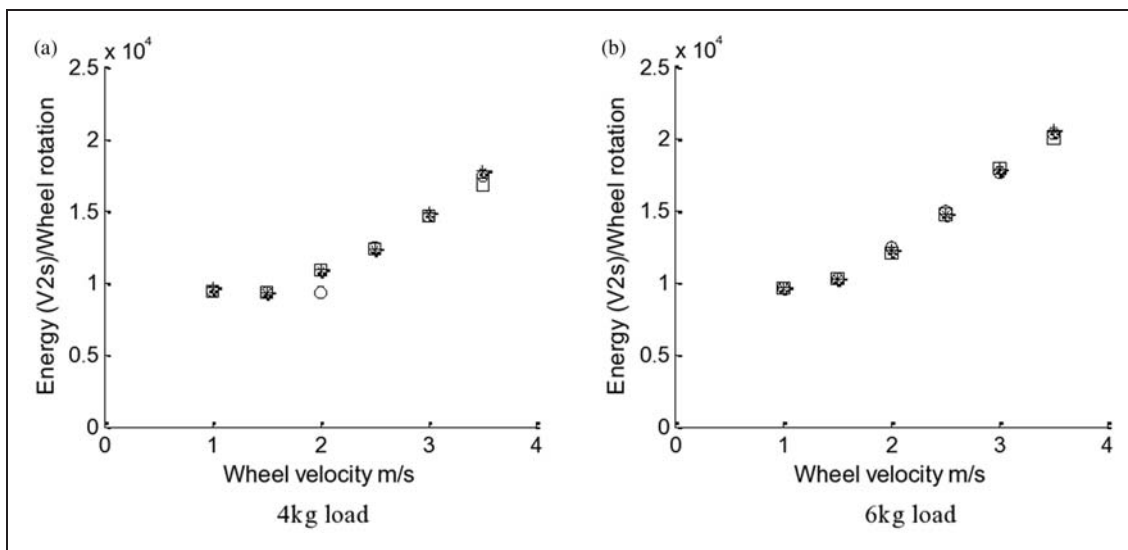


Figure 5. Effect of speed on energy per wheel rotation for (a) 4 kg load and (b) 6 kg load in tests with spacer installed.

the trigger sensor being placed nearer (0.1 m) to the joint in the track (Figure 1) so that recording started when the wheel hit the joint. For the wheel speeds used, the 2-s recording time corresponded to between 2 and 7 m circumferential progress of the wheel and the pre-trigger time was maintained constant at 0.04 s. Three 2-s records were taken for every wheel speed and load condition. PAC Micro-80D AE sensors

and PAC type 1220 A preamplifiers were used for measurement and trigger, and these were connected to an NI 6115 data acquisition board.

The wheel had a lateral float of 1.5 mm in the bearing housing which gave rise to lateral rattling, particularly at lower speeds and loads when there were lower normal and centrifugal forces. In the first set of experiments, the lateral float was reduced by

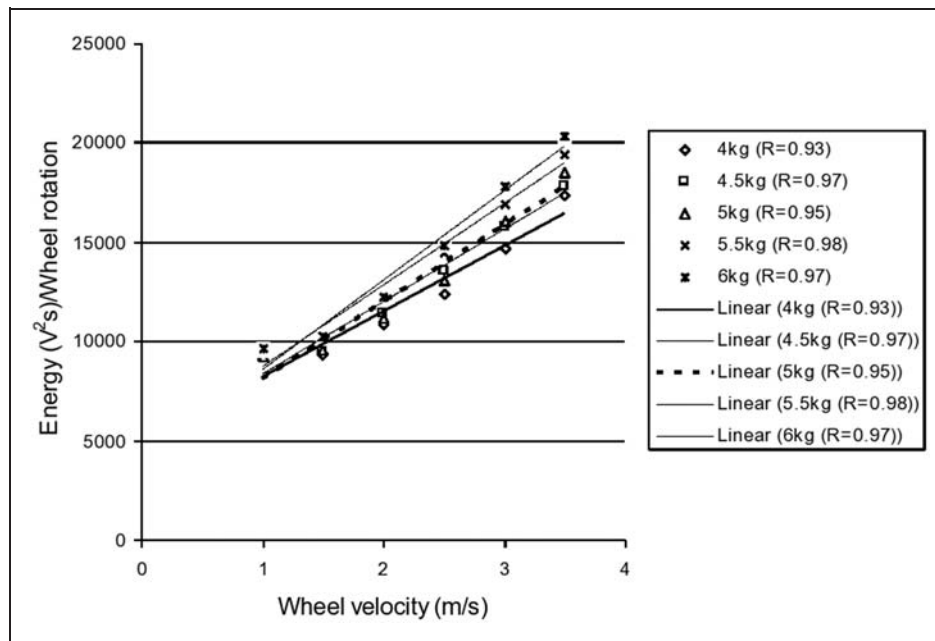


Figure 6. Effect of speed on mean energy per wheel rotation for all loads studied in tests with spacer installed.

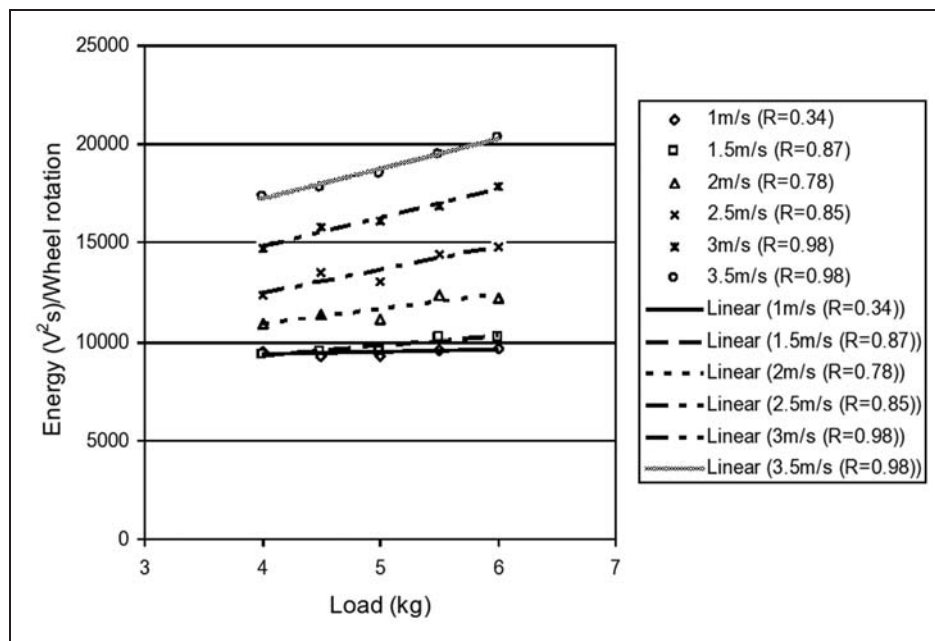


Figure 7. Effect of axle load on mean energy per wheel rotation in tests with spacer installed.

introducing a 1 mm spacer (Figure 4) on the flange side of the shaft. In the second set of experiments the spacer was not used and a slight eccentricity was built into the track by displacing the motor shaft by about 2.5 mm from the centre of the circular track. The effect of this was to cause rubbing between the wheel and flange over an arc between circumferential distances of 1.4 and 2.4 m from the joint.

With the spacer installed, six wheel speeds (1, 1.5, 2, 2.5, 3 and 3.5 m/s) were used with five different axle loads (4, 4.5, 5, 5.5 and 6 kg). With the spacer absent,

five wheel speeds were used (1, 1.5, 2, 3 and 3.5 m/s) with four axle loads (4, 5, 6 and 6.5 kg).

Because the wheel is moving relative to the sensor, it is necessary to take into account attenuation and to correct the intensity of the signal accordingly. A moving source model has been developed for this purpose (reported in detail in Thakkar et al.<sup>22</sup>), and this was applied to all records to yield a corrected time series as if the wheel was directly above the sensor. This was possible because the wheel produced a large spike in AE when crossing the joint so that its

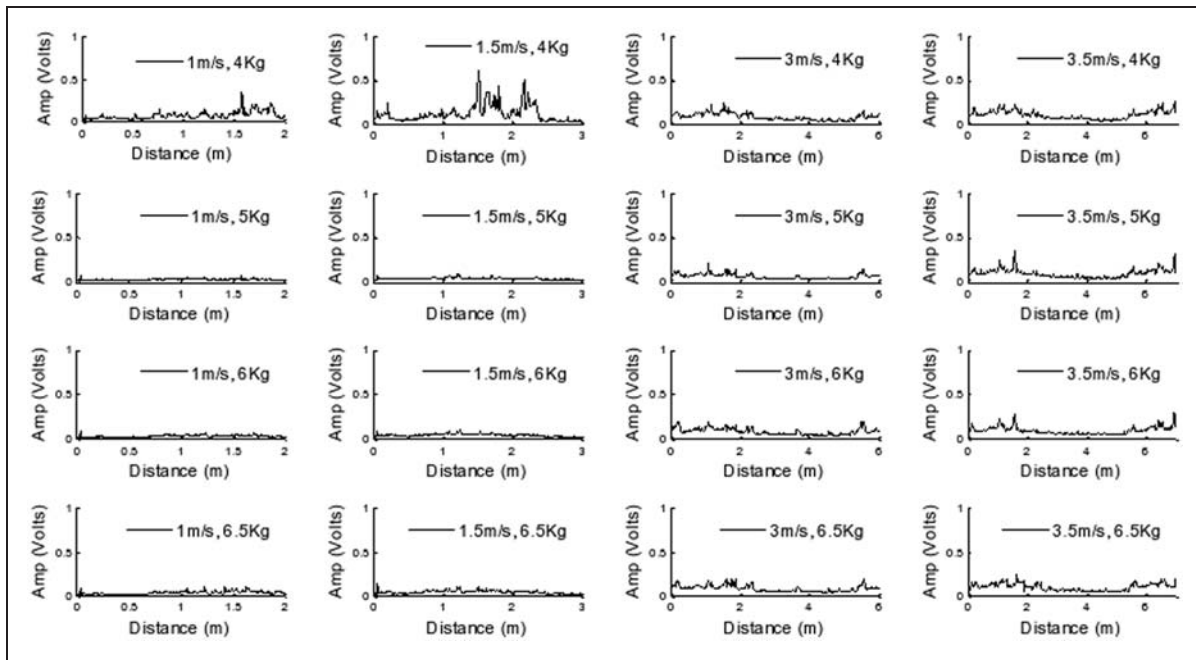


Figure 8. Effect of speed and load on AE records with spacer absent.

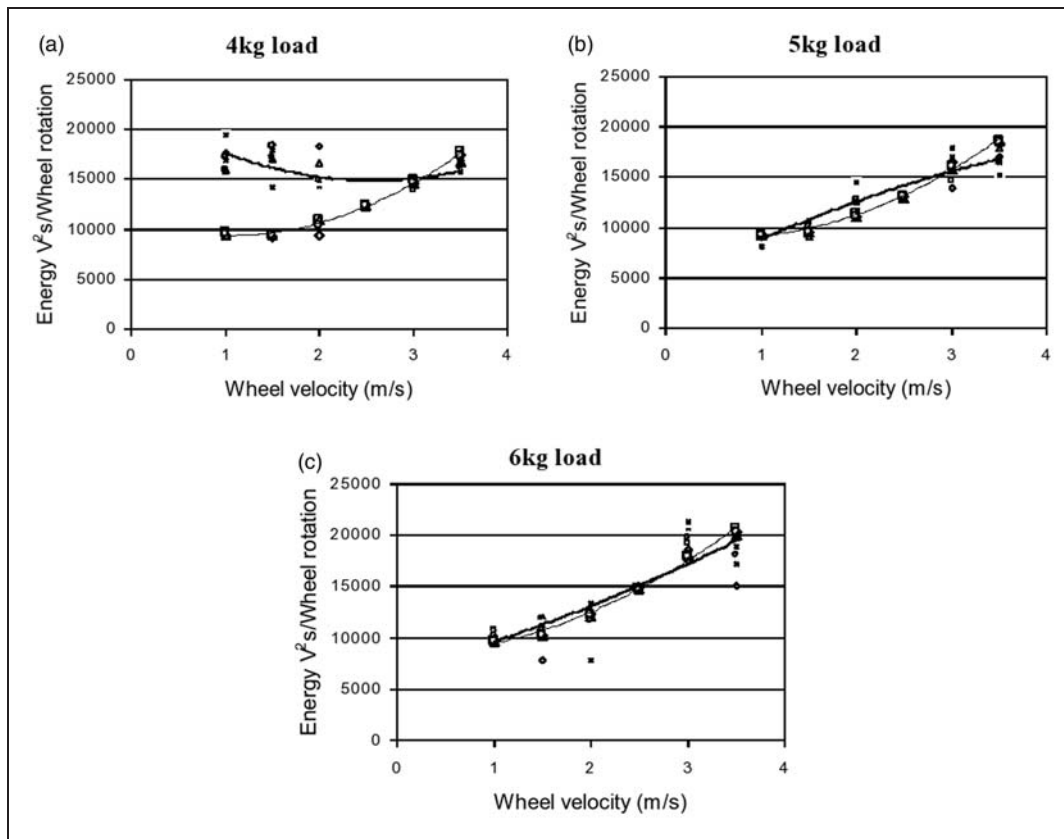
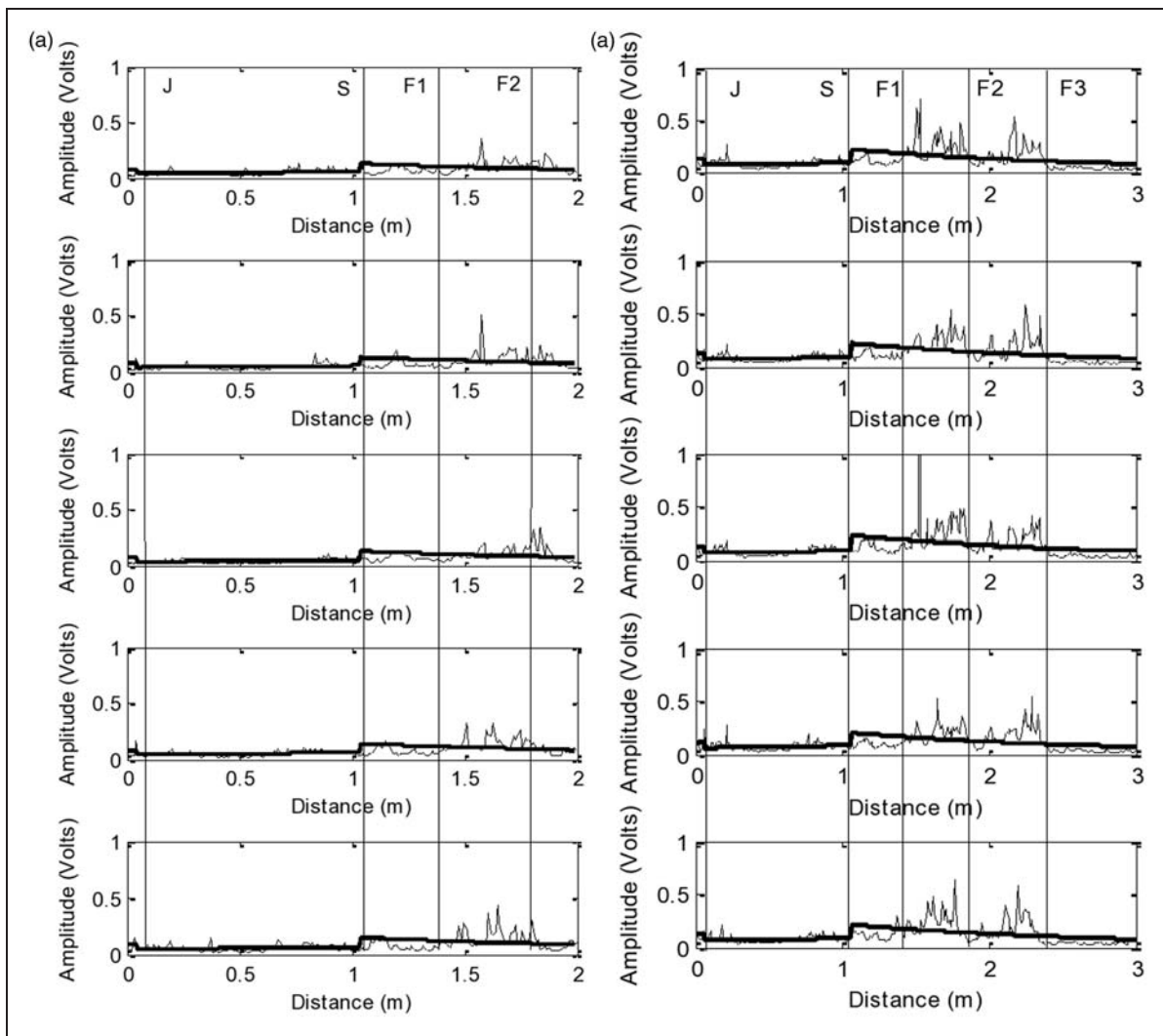


Figure 9. Effect of speed and load on energy per wheel rotation with (dotted polynomial fit line) and without (solid line) spacer: (a) 4 kg load; (b) 5 kg load; and (c) 6 kg load.



**Figure 10.** Measured RMS AE (light solid line) and analytical model (dark solid line) at 4 kg and wheel speed (a) 1 m/s and (b) 1.5 m/s. Dotted lines marked J and S are the positions where the wheel passes over the joint and sensor, respectively. The two areas of wheel flange rubbing are identified by the dotted lines F<sub>1</sub>, F<sub>2</sub> and F<sub>3</sub>.

circumferential position can always be found in the AE record, knowing the rolling speed.

### Effect of wheel speed and load without lateral rattling or flange rubbing

The energy per wheel rotation was calculated for the region commencing at 0.05 m from the joint, by taking the root mean square (RMS) of the record and integrating for a time corresponding to one rotation of the wheel (different times for a constant distance of  $0.09\pi$  m). The effect of speed on energy per wheel rotation is shown in Figure 5 for the two extreme values of load, and it appears that there is an approximately parabolic increase in energy with speed, with very little scatter between the three measurements at each speed and load. Figure 6 shows the effect of speed for the remaining loads and Figure 7 shows the effect of load for each speed, both plotted on a single graph with a linear fit to give a quantitative estimate of the speed and load increases.

It is clear from Figures 6 and 7 that the effect of speed on AE energy per wheel rotation is significantly greater than the effect of axle load. This result is somewhat unexpected, given the conventional wisdom on rail-track rolling resistance, although it has to be acknowledged that the track radius of curvature has not been scaled ~~in the work~~ in the way that the speed and load have in the experimental rig. This might account for the relatively large component of lateral force as identified by Zeng and Wu.<sup>11</sup>

### Wheel lateral rattling

Figure 8 shows a sample of RMS data (averaged over a 0.01 m distance) for one of the five 2-s records taken under each of the 16 conditions. As before, the signal level generally increases with speed and load (bottom right) but, in contrast to the tests with the spacer installed, the AE energy is also high at the lowest speeds and loads (top left).

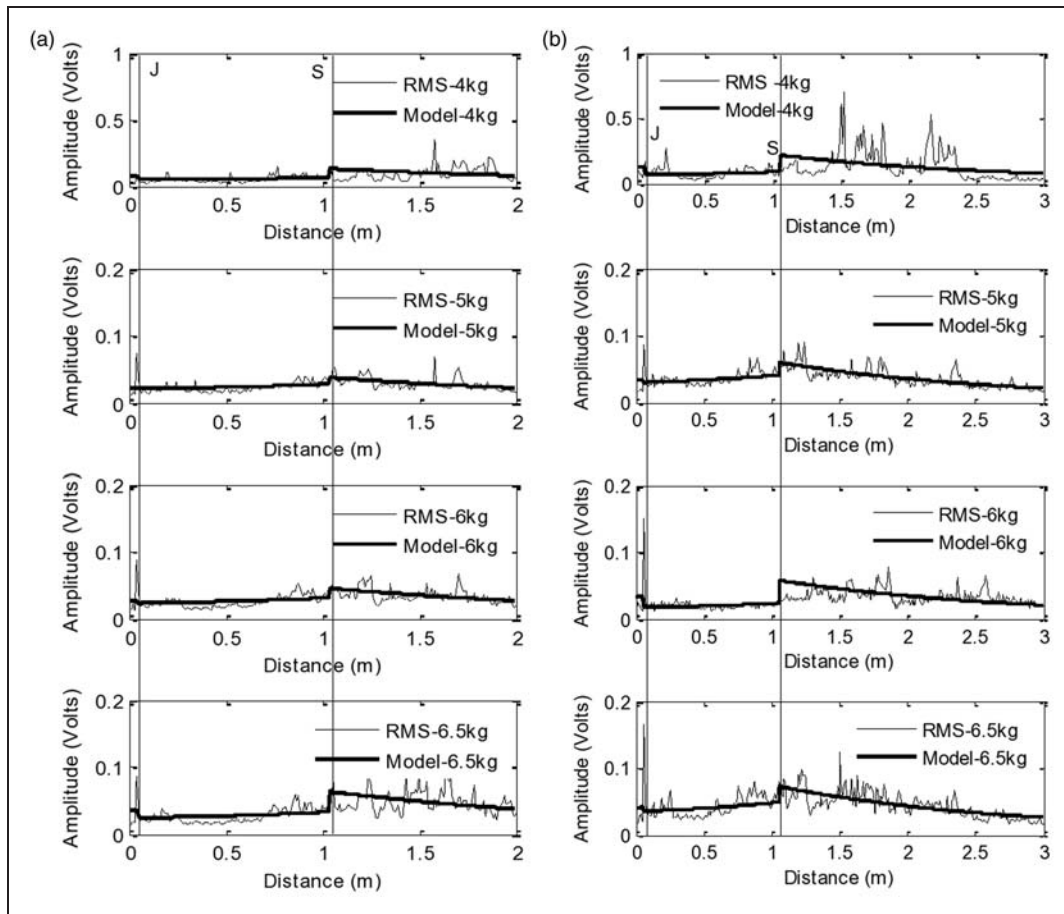


**Figure 11.** Measured RMS AE (light solid line) and analytical model (dark solid line) for one of the measurements for all loads and lower speeds (a) 1 m/s and (b) 1.5 m/s.

Figure 9 compares the effect of speed on the energy per wheel rotation with and without the spacer for the three common axle loads used. The polynomial fits are almost coincident except at the lowest load and, then, the divergence is greatest at the lower speeds. This anomalous effect is attributed to lateral rattling of the wheel, which is freer to move when the centrifugal contact force is smaller. The fact that the effect is diminished when the spacer is installed, along with the fact that it is observed with the combination of low speeds and loads, makes the explanation of vertical bouncing at low loads unlikely.

### Wheel flange rubbing

The built-in eccentricity in the tests without the spacer gave rise to flange rubbing at circumferential distances between 1.4 and 2.4 m clockwise from the joint (well beyond the  $0.09\pi$  m depicted in Figure 9). There were also some natural defects in the same area between 1.46 and 1.58 m although their effect has already been assessed.<sup>23</sup> In order to correct for along-track attenuation and to identify areas of the track where the AE was above 'normal' a moving source model<sup>22</sup> for the AE energy in short time-step averaged RMS signals was applied. This consisted of fitting two

attenuation curves to the data, one for the shorter section between joint and sensor and one for the longer one

$$\begin{aligned}
 E_t &= E_0 e^{-kx_1} + RE_0 e^{-k((c_2-x_1)+c_2)} \\
 &\quad + RE_0 e^{-k(c_1-(c_2-x_1)+(c_1-c_2))} \\
 &\quad + TE_0 e^{-k(c_1-x_1)} + TE_0 e^{-k(c_1+x_1)} \\
 E_t &= E_0 e^{-kx_2} + RE_0 e^{-k(x_2+c_2+c_2)} \\
 &\quad + RE_0 e^{-k(c_1-(c_2+x_2)+(c_1-c_2))} + TE_0 e^{-k(c_1-x_2)} \\
 &\quad + TE_0 e^{-k(c_1+x_2)}
 \end{aligned}$$

where  $E_t$  is the energy at a clockwise distance,  $x_1$ , or anticlockwise distance,  $x_2$ , from the joint,  $R$  and  $T$  are the reflection and transmission coefficients at the joint,  $k$  is an exponential attenuation coefficient, and  $c_1$  and  $c_2$  are the clockwise and anticlockwise distances of the sensor from the joint. Since  $R$ ,  $T$  and  $k$  have been measured in a calibration using pencil-lead breaks, the curve-fitting is a simple matter of obtaining the best value of  $E_0$ , the mean source energy (effective energy of the source when directly above the sensor), taking into account the entire record of AE.

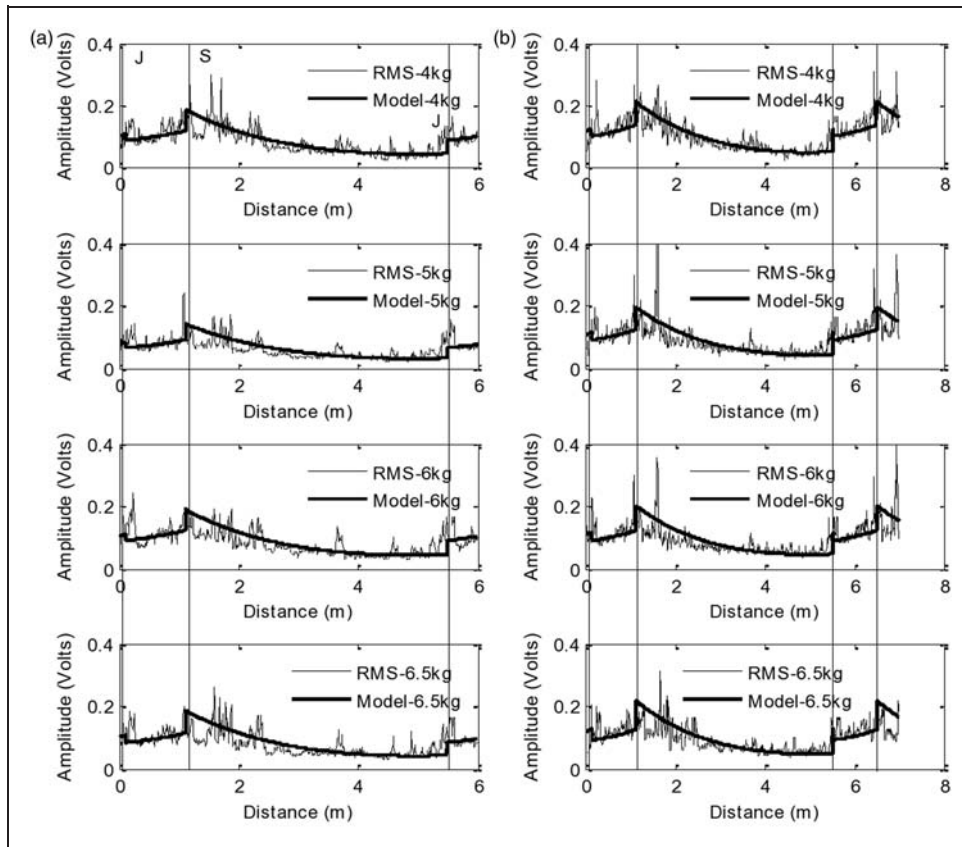


**Figure 12.** Measured RMS AE (light solid line) and analytical model (dark solid line) for one of the measurements for all loads and higher speeds (a) 3 m/s and (b) 3.5 m/s.

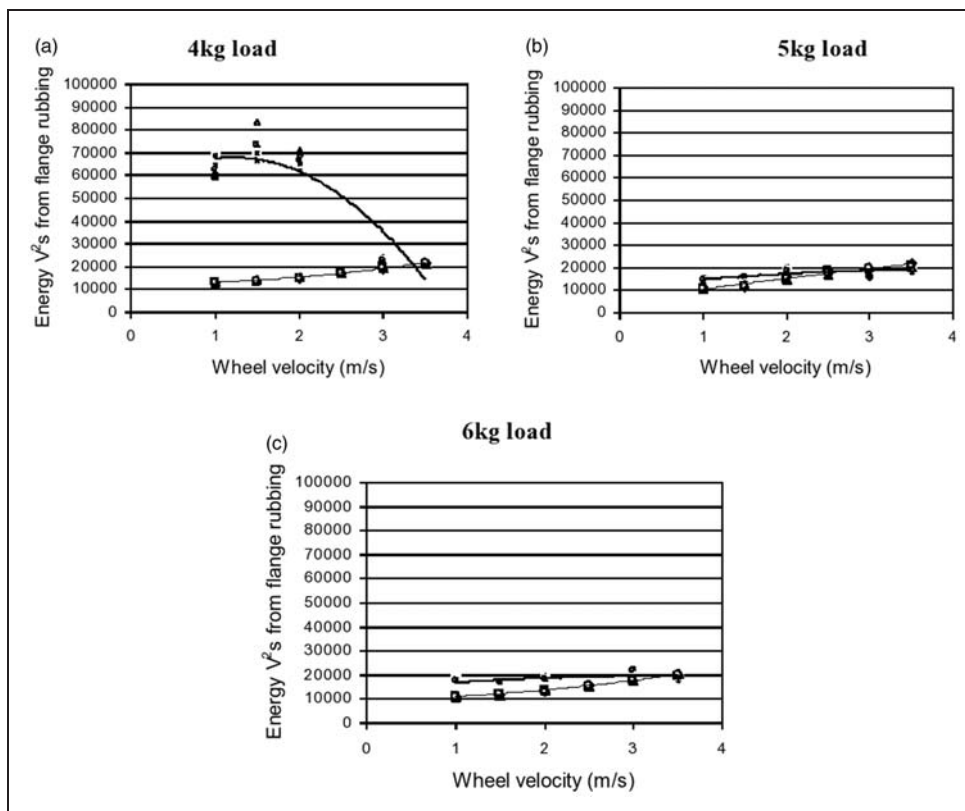


**Figure 13.** Effect of speed and load on energy per wheel rotation in the flange rubbing arc with (dotted polynomial fit line) and without (solid line) spacer and track eccentricity: (a) 4 kg load; (b) 5 kg load; and (c) 6 kg load.

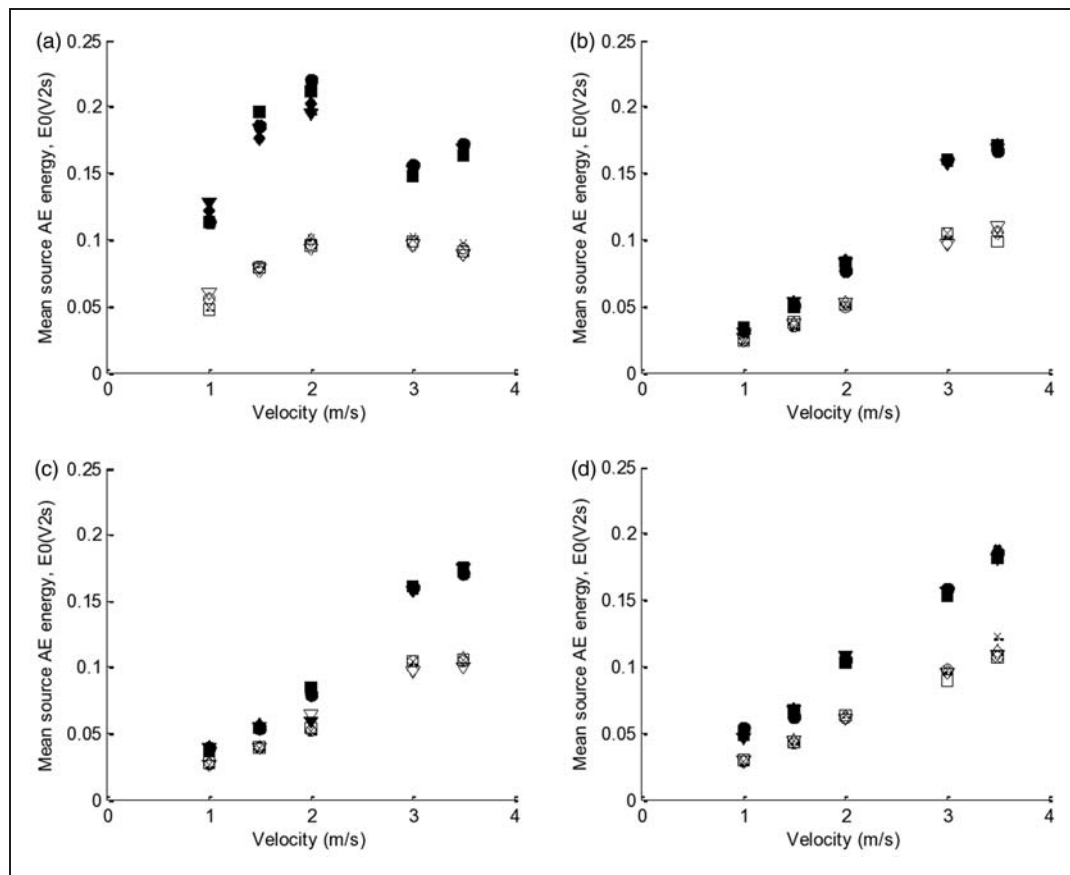


**Figure 14.** Effect of speed and load on mean source energy for wheel moving away from sensor (solid symbols) and for wheel approaching sensor (open symbols).

Figure 10 shows the five full records for the low load and lower speeds along with the best-fit analytical model, demonstrating that the experiment is quite repeatable, even in these less stable conditions, but also showing that the signal is above the attenuation curve in the area of flange rubbing. Figures 11 and 12 show examples of data with the fitted analytical model for each of the speeds and loads studied.

### Cumulative effect of wheel rattling and flange rubbing

The AE energy was calculated for flange rubbing by integrating over the arc of rail-wheel contact and dividing by the number of wheel rotations in the arc. The result is shown in Figure 13, plotted against wheel speed in comparison with the corresponding arc with no rattling or flange rubbing for the common loads studied. At higher loads, the flange rubbing introduces an increase of between 50 and 75%, the difference decreasing as the speed increases, whereas, at the lowest speed, this increase is more like a factor of seven to eight, again decreasing as the speed increases. Thus, the rattling effect is considerably increased in the area of flange rubbing.

### Effect of speed and load on mean source energy

Figure 14 shows the 10 values of  $E_0$  (five from rising curves and five from falling curves) for each speed and load. The mean source energy increases approximately linearly with wheel speed, but with different slopes for the rising and falling curves. The exception to this is for the lightest load where the mean source energy values for the falling curves are approximately two to three times higher than the rising values for speeds less than or equal to 2 m/s, Figure 14(a), and this effect is attributable to lateral wheel rattling and wheel flange rubbing.

### Locating abnormal rail-wheel contact

The value of RMS AE above normal rolling background (as defined by the model) was averaged per 0.1 m length of track over each of the five records, and is shown in Figure 15(a) for one set of rolling conditions. The lengths of all natural defects on the track running surface were measured and a map was prepared of the total length of defect per 0.1 m length of track, normalized to the highest value recorded, yielding the intensity map shown in Figure 15(b).

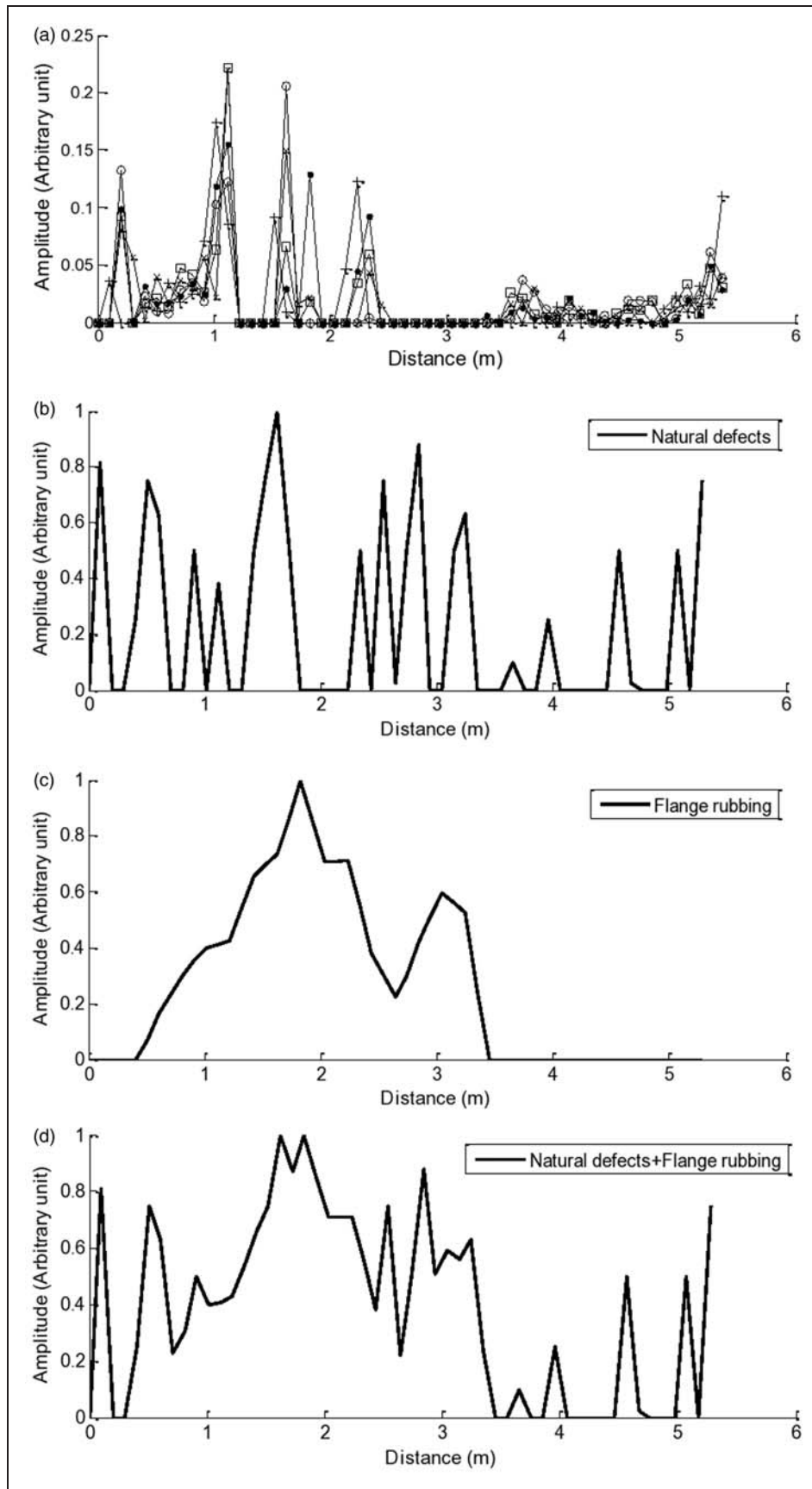


**Figure 15.** Track AE and defect maps for wheel speed of 3.5 m/s and 5 kg load: (a) signal above normal rolling, (b) intensity for natural defects, (c) intensity for flange rubbing and (d) combination of natural defect intensity and flange rubbing.

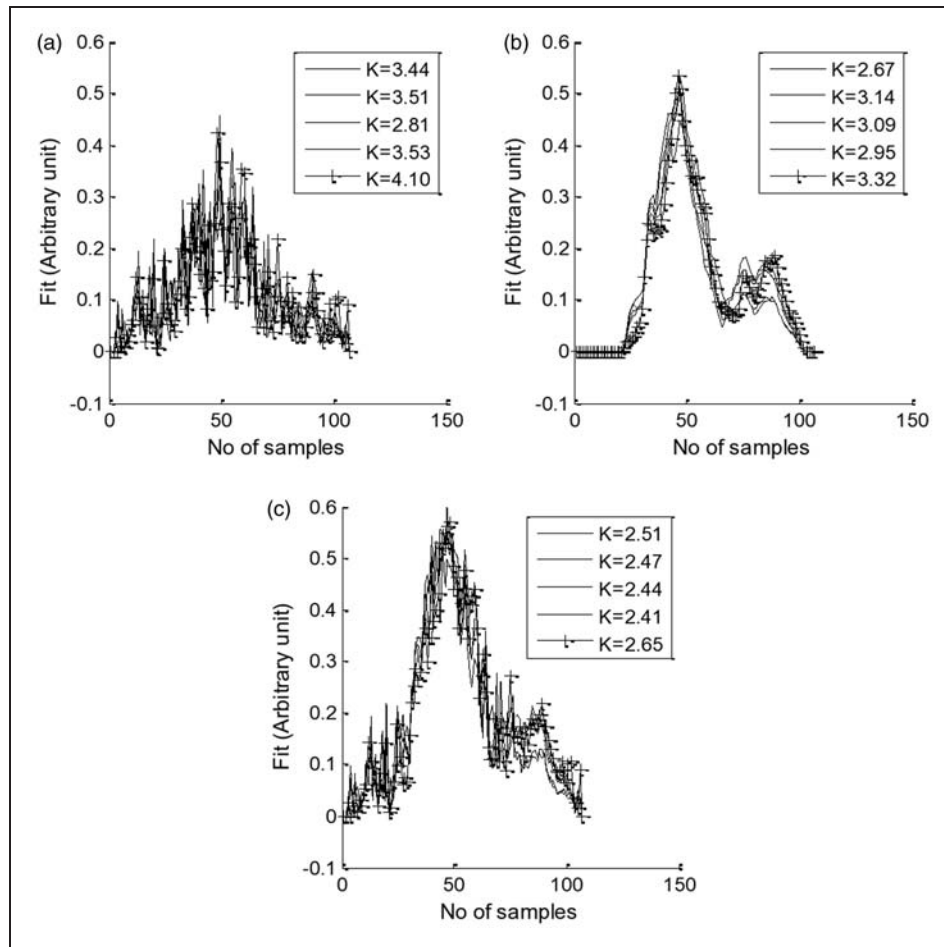


**Figure 16.** Cross-correlation between AE above normal rolling and defect intensity from: (a) natural defects; (b) flange rubbing; and (c) natural defects with flange rubbing for a wheel speed of 3.5 m/s and 5 kg load condition.

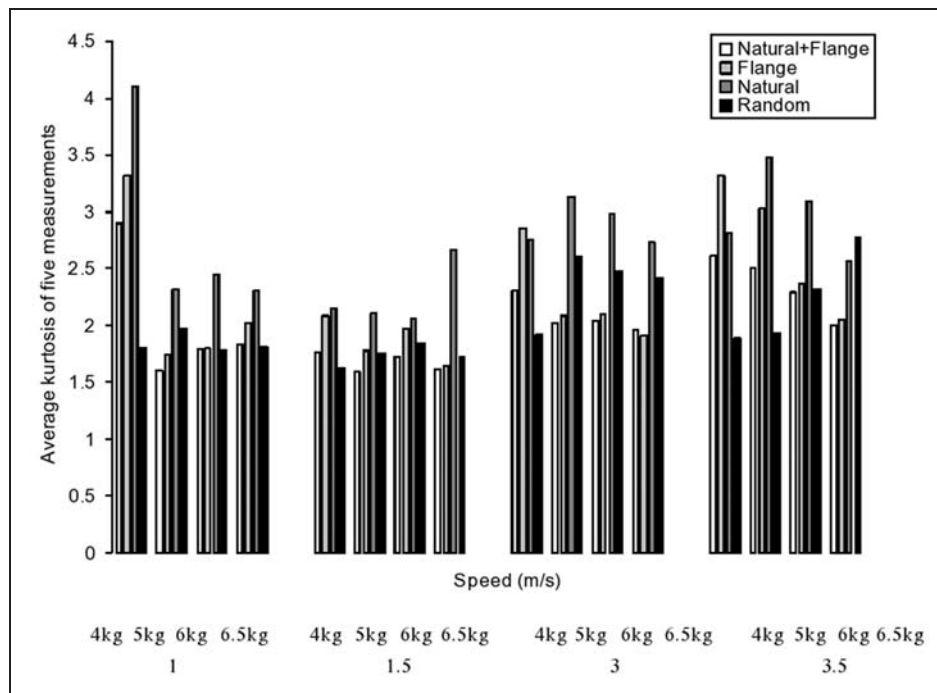


**Figure 17.** Average kurtosis of cross-correlation function between track defects and AE above normal rolling background for all experiments with no spacer installed.

Finally the degree of eccentricity of the track was also calculated per 0.1 m length and a normalized map of rubbing intensity prepared as shown in Figure 15(c). Figure 15(d) shows the two defect intensities added together and re-normalized.

In order to assess the extent to which the AE energy above normal rolling was sensitive to flange rubbing, natural defects, or both, each of the maps shown in Figures 15(b), (c) and (d) were cross-correlated with the AE RMS above normal rolling, Figure 15(a). The relevant cross-correlation functions (normalized to give unit area) are shown in Figures 16 (a), (b) and (c), respectively, ~~Figure 16~~ for the rolling conditions depicted in Figure 15. In the interest of having a single indicator of the strength of the cross-correlation, the kurtosis of the normalized cross-correlation function was calculated, as giving a measure of its peakedness. Although kurtosis can be more accurately described in terms of the lengths of the distribution tails and modality as well as peakedness<sup>27,28</sup>, for the shapes depicted here, a higher kurtosis can be considered to correspond to a more 'pointed' cross-correlation function, i.e. better correlation between AE and defect severity distribution).

The average kurtosis values are 3.48, 3.03 and 2.5 for AE correlation with natural defects, flange rubbing and both defects, respectively. Figure 17 shows the result of applying the same approach to the 16 different conditions of wheel speed and axle load giving the average kurtosis of the five measurements at each condition for the natural defects, the flange rubbing, the combination of natural defects and flange rubbing, and a randomly generated defect severity map. It can be seen that, in most conditions, the natural defects give better correlation than any of the other maps, despite the fact that the natural defects are much more widely distributed around the track than is the flange rubbing. In only one case did the randomly generated defect severity map lead to better correlation than the natural defects, and in only two did the flange rubbing map give better correlation than the natural defects.

## Conclusions

The experiments with inhibited lateral rattling (normal rolling) have revealed that the AE energy per wheel rotation increases in an approximately linear fashion with axle load and in an approximately quadratic fashion with wheel speed. It is expected that the speed effect is due to centrifugal force so that the normal rolling experiments would indicate that the AE energy per wheel rotation increases with contact force in the same way as does the wheel frictional resistance.

The experiments where lateral rattling was not inhibited have shown that the frictional instability at lower axle loads and speeds shows up in the AE

record, suggesting that AE will also be sensitive to frictional instability in real rails.

Flange rubbing and natural rail defects are both detectable in the AE record. A method using cross-correlation between the AE signal above the normal rolling threshold and the defect severity has shown both types of defect to be detectable, but the natural defects give a greater enhancement of AE energy than does flange rubbing.

Overall, the work shows that the conditions leading to wheel and track degradation can potentially be monitored using acoustic emission. Application to real rail assets would require sensors to be deployed on working track with records being made of the AE generated by a series of train passings, where the details of the actual trains could also be recorded (speed, axle load, and wheel and track conditions). Such a 'calibration' would then allow continuous monitoring of the part of the track on which the sensors were deployed and, if the area were to be well-chosen, additional information to be provided for asset management.

## Funding



## References

1. Tournay HM. A future challenge to wheel/rail interaction analysis and design. *Wear* 2008; 265: 1259–1265.
2. Öberg J and Andersson E. Determining the deterioration cost for railway tracks. *Proc IMechE, Part F: J Rail Rapid Transit* 2009; 223: 121–129.
3. Thompson DJ and Jones CJC. A review of the modelling of wheel/rail noise generation. *J Sound Vib* 2000; 231(3): 519–536.
4. Kalker JJ. Survey of wheel-rail rolling contact theory. *Veh Syst Dyn: Int J Veh Mech Mobility* 1979; 8(4): 317–358.
5. Tunna J, Sinclair J and Perez J. A review of wheel wear and rolling contact fatigue. *Proc IMechE, Part F: J Rail Rapid Transit* 2007; 221: 271–289.
6. Evans JR, Lee TKY and Hon CC. Optimising the wheel/rail interface on a modern urban rail system. *Veh Syst Dyn: Int J Veh Mech Mobility* 2008; 46(1): 119–127.
7. Wu H, Kalay S and Tournay H. Development of the wheel-rail interface management model and its applications in heavy haul operations. *Proc IMechE, Part F: J Rail Rapid Transit* 2011; 225: 38–47.
8. Storhaug G, Moe E and Holtmark G. Measurements of wave induced hull girder vibrations of an ore carrier in different trades. *Trans ASME, J Offshore Mech Arctic Engng* 2007; 129: 279–289.
9. American Railway Engineering and Maintenance-of-Way Association. *AREMA manual for railway engineering*. Lanham, MD: AREMA, 2011, pp.16-2-2–16-2-9.
10. Lukaszewicz P. Running resistance and energy consumption of ore trains in Sweden. *Proc IMechE, Part F: J Rail Rapid Transit* 2009; 223: 189–197.
11. Zeng J and Wu P. Stability analysis of high speed railway vehicle. *JSME Int J, Series C* 2004; 47(2): 464–470.



12. Kim J-K and Kim C-S. Fatigue crack growth behavior of rail steel under mode I and mixed mode loadings. *Mater Sci Engng A, Struct Mater, Prop Microstruct Process* 2002; 338: 191–201.
13. Akama M and Nagashima T. Some comments on stress intensity factor calculation using different mechanisms and procedures for rolling contact fatigue cracks. *Proc IMechE, Part F: J Rail Rapid Transit* 2009; 223: 209–221.
14. Sandström J and Ekberg A. Predicting crack growth and risks due to wheel flat impacts in heavy haul operations. *Proc IMechE, Part F: J Rail Rapid Transit* 2009; 223: 153–161.
15. Kumar S, Espling U and Kumar U. Holistic procedure for rail maintenance in Sweden. *Proc IMechE, Part F: J Rail Rapid Transit* 2008; 222: 331–344.
16. Papaelias MP, Roberts C and Davis CL. A review on non-destructive evaluation of rails: state-of-the-art and future development. *Proc IMechE, Part F: J Rail Rapid Transit* 2008; 222: 367–384.
17. Pau M and Leban B. Ultrasonic assessment of wheel-rail contact evolution exposed to artificially induced wear. *Proc IMechE, Part F: J Rail Rapid Transit* 2009; 223: 353–364.
18. Attivissimo F, Danese A, Giaquinto N and Sforza P. A railway measurement system to evaluate the wheel-rail interaction quality. *IEEE Trans Instrum Meas* 2007; 56(5): 1583–1589.
19. Shiroishi J, Li Y, Liang S, et al. Bearing condition diagnostics via vibration and acoustic emission measurements. *Mech Syst Signal Process* 1997; 11(5): 693–705.
20. Bruzelius K and Mba D. An initial investigation on the potential applicability of acoustic emission to rail track fault detection. *NDT & E Int* 2004; 37: 507–516.
21. Thakkar NA, Steel JA, Reuben RL, et al. Monitoring of rail-wheel interaction using acoustic emission (AE). *J Adv Mater Res* 2006; 13-14: 161–167.
22. Thakkar NA, Steel JA and Reuben RL. Mapping of wheel flange rubbing on rail using AE: laboratory test. *J Acoust Emiss* 2007; 25: 348–354.
23. Thakkar NA, Reuben RL and Steel JA. Rail-wheel interaction monitoring using acoustic emission: a laboratory study of normal rolling signals with natural rail defects. *Mech Syst Signal Process* 2010; 24(1): 256–266.
24. Thakkar NA, Steel JA and Reuben RL. Rail-wheel contact stress assessment using acoustic emission: a laboratory study of the effects of wheel flats. *Proc IMechE, Part F: J Rail Rapid Transit* [in press](#).
25. Armstrong TD and Thompson DJ. Use of a reduced scale model for the study of wheel/rail interaction. *Proc IMechE, Part F: J Rail Rapid Transit* 2006; 220: 235–245.
26. Pilkey WD. *Stress, strain and structural matrices*. New York: Wiley, 2004.
27. Darlington RB. Is kurtosis really peakedness? *Am Stat* 1970; 24(2): 19–22.
28. DeCarlo LT. On the meaning and use of kurtosis. *Psychological Methods* 1997; 2(3): 292–307.